Mechanisms and kinetics during reactive infiltration of molten silicon in porous graphite

J. Roger [a]*, G. Chollon [a]

[a] Université de Bordeaux, CNRS, Laboratoire des Composites ThermoStructuraux, UMR 5801, 33600 Pessac, France

* Corresponding author: e-mail: jerome.roger@lcts.u-bordeaux.fr

Abstract

Liquid silicon Infiltration (LSI) is a fast and economical process to manufacture SiC-based ceramics. For a better understanding of reactive melt infiltration of liquid silicon, the wetting and infiltration of porous graphite by molten silicon were investigated at 1450, 1500 and 1550°C for duration comprised between 10 s and 1 h. Infiltrations tests were performed in an argon atmosphere with an inductively heated furnace operating with heating and cooling rates of 300°C.min^{-1}. The formation and growth of SiC grains were investigated at the outer surface and within graphitic carbon substrates with 11% porosity and a narrow pore size distribution centered at 2 μm. The length of the infiltrated zone and the SiC crystals growth were determined from scanning electron microscopy. Rapid spreading and infiltration of molten silicon are observed from the first 60 seconds. The growth rate of the interfacial SiC layer obeys a fourth-power law with an activation energy of 260±30 kJ.mol^{-1}. Pore filling by SiC is limited by volume diffusion with an activation energy equal to 320±40 kJ.mol^{-1}.

Keywords: A Grain growth; B Composites; B Electron microscopy; D Carbon; D SiC; E Refractories

1. Introduction

Silicon Carbide (SiC) is one of the most important advanced ceramic, due to its unique set of properties: wide band gap, good oxidation resistance, high thermal stability and conductivity, low density and high toughness [1-4]. The potential applications of this material include components for advanced propulsion systems, energy conversion devices, and other high-temperature structures. A wide range of processes was developed for the synthesis of SiC-based materials [5,6]. The main barrier nowadays in the fabrication of silicon carbide-based ceramics is related to complex shape fabricability, processing time, temperatures, pressure, and control of the final product quality. A combination of these factors leads to higher manufacturing cost of the final components. Owing to the above considerations, there is a strong need to develop alternative processing approaches for silicon carbide-based advanced ceramics. Out of all the procedures available, liquid-phase reactive infiltration has proven to be the most promising to obtain almost non-porous and large SiC pieces. During the liquid silicon infiltration (LSI) of a carbon porous preform, silicon readily reacts with the carbon skeleton during the infiltration to produce SiC [5,7-10]. The benefits are a minimization of the working temperature and processing time while improving the product quality and the shape control. According to the literature, the process of silicon infiltration and reaction with carbon is not satisfyingly understood [11-18]. The reaction between molten silicon and carbon complicates the infiltration and conversion process mainly because of its exothermicity and the permeability reduction implied by SiC formation. The exothermicity of the reaction was indeed assumed to generate a self-propagating high-temperature synthesis (SHS) with repeating successive carbon dissolution and SiC precipitation steps [13]. It was also found that the infiltration kinetics is influenced by both the pore morphology and size and the C-Si reaction, which decreases the effective pore radius slowing the infiltration rate [19-21]. If the pore size is too small or presents a typical ink bottle shape, the pore may even be closed or become inaccessible during the reaction. Liquid silicon-carbon interaction was examined by several authors which concluded that: 1) liquid silicon readily wets carbon and the wetting is

enhanced by the SiC formation [22-25]; 2) coarse micrometric SiC crystals grow by dissolution of early-formed SiC nanocrystallites [26-28], and 3) the growth of a SiC layer implies also a limitation of the reaction by solid state diffusion [29,16]. Further additional features must be taken into account, such as the nature of carbon (amorphous or graphitized, grain size and structure), which affects its reactivity [30]; the working conditions (composition, temperature, pressure, time), which define several important parameters (liquid's viscosity, contact angle, surface tension, reaction rate constant) and consequently the dynamics and mechanisms of the liquid infiltration and the Si-C reaction [19]. Depending on these numerous parameters, the infiltration and conversion can be completed or only partial. Despite these numerous previous works, the development of LSI process requires more detailed investigations on the kinetics and mechanism involved, through: 1) the liquid silicon infiltration; 2) the SiC growth at the surface and within the preform. The approach of this work consists in studying a model system especially for short heating durations to verify the above assertions and to obtain more detailed data on this system with the aim of reaching a better understanding and control of the process. The dynamics of reactive infiltration of porous graphitic carbon by molten silicon was experimentally monitored at 1450, 1500 and 1550°C for durations up to 1 hour in order to establish the kinetics of the various steps of the process 1) the parabolic infiltration rate; 2) the growth of SiC at the surface; and 3) the pores closure. The aim is also to determine the corresponding Arrhenius activation energies and to identify the limiting steps of the process.

2. Materials and experimental procedures

The reactive infiltration of liquid silicon with solid carbon was examined on 4x4x3mm^3 carbon samples. All the faces of the carbon samples, excepted the upper one, were covered with a boron nitride (BN) layer to limit spreading of the liquid along the other faces. This protective layer was applied on the sides of carbon samples by spraying (HeBoCoat 21E,

Henze Boron Nitride Products AG, Germany). The experiments were performed on grade 2333 polycristalline graphite supplied by Mersen company (France). According to Figure 1-a), this carbon grade has a porosity of 11±1% with a mean pore size of 2 μm and a narrow distribution of the pore size. The pore size distribution was measured by mercury porosimetry on the samples characterized by helium pycnometry (Autopore IV, Micromeritics Instrument Corp., USA). This grade is totally graphitic with a grain size of 5 μm as shown in Figure 1-b). The XRD analysis was performed in the Bragg-Brentano geometry with a Bruker D8 Advance diffractometer using a Cu Kα radiation fitted with a one-dimensional position sensitive silicon strip detector (Bruker, Linxeye). The XRD pattern was recorded using a 2θ step size and range of respectively 0.01° and 10-100° and a counting time of 0.3 second per step. This carbon material was chosen as a model material because of: 1) its convenient and homogeneous pore size, 2) its weak porosity which is favorable to the analysis of phenomenons occurring in the pores while limiting the global exothermic effects. The liquid silicon used in this study was prepared by melting pure Si chips (99.9999 wt%, Strem Chemicals Inc, USA), with a total weight of 16±3 mg, on the uncoated carbon face previously polished down to 1 μm, as represented in Figure 2. The heating treatments of the pellets at 1450, 1500 and 1550°C were performed in an inductively heated graphite susceptor with heating and cooling rate of 300°C.min^{-1}. A continuous flow of high purity argon (Alphagaz 2, from AirLiquide) under normal pressure was applied to prevent oxygen pollution. After cooling, the cross-section of the samples was cross-cut and polished drown to a 1 μm diamond finish. The microstructures of the silicon-wet and silicon-infiltrated areas of the samples were examined with a FEI Quanta 400FEG scanning electron microscopy (SEM) operated at 5 kV. From backscattered-electron (BSE) micrographs and Image Analysis System (ImageJ) [31], it was possible to estimate the depth of the infiltration fronts, the thicknesses of the SiC and the different layers at the silicon-carbon interface; and the pore closure. The Raman analyses were performed with a Labram HR (Horiba Jobin Yvon) microspectrometer (λ = 632.8 nm, spectral resolution ≈2 cm^{-1}) in the punctual mode. The

lateral resolution is of the order of 1 µm but the depth probed can vary up to 3 µm in Si, depending on the purity. The incident power was kept below 1 mW to avoid local heating of the sample.

3. Results and discussion

3.1 Infiltration front in porous graphite

The progress of the infiltration front and the contact angles, was measured from metallographic sections, are presented in Figure 3 and Figure 4-a. The evolution of the contact angle at 1450°C is in good agreement with that reported by O. Dezellus et al. at 1430°C [22] or by N. Eustathopoulos et al. at 1460°C [25]. For all temperatures, a rapid decrease of the contact angle is observed. The values are lower than 20° after only 600 s and, remain stable, taking into account the uncertainty of the measurements. It is worth noting that at 10 and 60 s, the angle is mower at 1550°C than at 1450°C; at 600 s the opposite situation is observed. The behavior at 1500°C is particular: a strong decrease is measured between 10 and 60 s and the contact angle decreases very slowly at 300 and 600 s compared to the two other temperatures. These observations are probably related to the reactivity and the infiltration processes. The infiltration depth of molten silicon was measured for all the samples from image analysis. The measured values are shown in Figure 4-b. The progress of the infiltration front is very rapid during the first 60 seconds and slows down for longer durations, reaching a nearly constant thickness of about 870 μm, 1170 μm and 1020 μm at 1450, 1500 and 1550°C, respectively. As previously reported from mathematical models describing the LSI process [11,21,32,33,34], the infiltration depth is found logarithmically dependant on time for the shortest durations as shown in Figure 4-c. This relationship applies very well at 1450 and 1550°C but is less acceptable at 1500°C due to the deeper infiltration measured at this temperature. This particular behavior could be induced by the exothermicity of the reaction acceleration of the kinetics of the liquid flow within the pores. This phenomenon could

explain that the infiltration length at 60 seconds is close to the value at 1550°C for the same duration. The variation of the apparent penetration kinetics of the liquid was also estimated and represented in Figure 4-d. For all temperatures, the apparent infiltration rate decreases very rapidly versus time to a nearly negligible value beyond 1200 seconds. Despite the elevated heating rate, evolutions may occur during the 6, 16 and 26 seconds needed to reach the plateau temperatures of respectively, 1450, 1500 and 1550°C from the silicon melting point (1420°C). Since these different regimes probably affect the experimental data, the instantaneous kinetic was not calculated.

3.2 Graphite/drop interfacial reaction zone

Figure 5 shows BSE micrographs of the cross-sections of the samples produced at 1450°C at different duration times: 10 s (Fig. 5-a), 60 s (Fig. 5-b), 300 s (Fig. 5-c), 600 s (Fig. 5-d). On these images, no reaction layer appears at the solid/liquid interface at the outer surface of the porous graphite for the short durations, i.e. 10 and 60 s. Isolated SiC grains start to form and grow for longer durations, resulting in a thick and continuous layer after 600 s. The same behavior was identified for the two other considered temperatures. Despite the absence of a continuous SiC layer, the silicon drop rapidly wets the surface of the carbon sample, in agreement with the work of O. Dezellus et al. reporting that liquid silicon readily wets solid carbon even in the absence of an interfacial SiC layer [22,24]. Some SiC grains are visible in Figure 5-a, although in very low amount, most of them having probably precipitated during the cooling from the supersaturated liquid. The wetting is further enhanced by the formation of a SiC layer with a contact angle of about 35°. The formation of this layer is delayed because it can only occur when the liquid is carbon-saturated. The interfacial reaction layer is composed of two sub layers, as shown in the inset in Figure 5-c. The layer close to the carbon substrate is commonly called Layer I. As previously reported [18,28], this layer most probably consists of nanometric SiC crystals involving a high density of stacking faults and dispersed in molten silicon. From EDS analysis, the chemical composition of this layer was

found to evolve gradually with time and temperature from the atomic ratio Si:C = 7:3 (1450°C/300s) to 1:1. The layer in contact with the liquid, called Layer II, is irregular since composed of faceted SiC crystals of variable size with local traces of silicon in the space between the SiC grains. Because of the growth of Layer II, Layer I disappears progressively, as shown in Figure 5-d where this layer is no longer continuous. For B. Mainzer et al., the driving force for the large SiC crystals growth is the elimination of stacking defects by grain coarsening [28]. The evolution of the thicknesses of these two layers was measured from BSE images and the so-obtained values are plotted in Figures 6-a and 6-b. The thicknesses of Layer II were obtained with help of ImageJ software to measure the areas corresponding to the SiC crystals and by converting this value to an equivalent and continuous SiC layer. The thicknesses of Layer I reach almost constant values after only a few minutes up to about 20 minutes. These values depend on the temperature, a higher temperature promoting a thicker layer. For high durations of at least 180 seconds, larger thicknesses are observed, but they correspond to areas where Layer I is still present (dotted lines in Figure 6-a). Indeed, this layer is progressively converted into practically pure SiC until becoming indiscernible of Layer II, in accordance with the observations reported previously [18]. H. Zhou and R.N. Singh studied the growth kinetics of a continuous SiC layer at the surface of glassy carbon. These authors reported that a weakened growth of the equivalent thicknesses of Layer II is observed, which is found to obey a fourth-power rate law corresponding to Equation 1 [29] (with correlation coefficients being at least equal to 0.94):

$$d_{II}^4 = k_{II}(T).t \qquad \text{Equation 1}$$

where d_{II} is the equivalent thickness of Layer II, $k_{II}(T)$ the kinetic coefficient ($\mu m^4.s^{-1}$) at the temperature T, and t the time. The parabolic and linear-parabolic laws are not suitable, as reported by the same authors [29]. However, it is worth noting that this fourth-power rate law is only valuable for durations up to 1800 s at 1450°C and only up to 1200 s at 1500 and 1550°C. The thickness indeed seems to reach a nearly constant value beyond these durations. This feature could be correlated to the disappearance of Layer I. The growth of Layer II seems

to be mainly dependent on the existence of Layer I. One can consider that Layer I promotes the diffusion of carbon atoms and consequently the growth of SiC crystal within Layer II. The Arrhenius plot, presented in Figure 6-d, was drawn on the basis of the logarithmic form of the kinetic coefficient as expressed by Equation 2:

$$Ln(k_{II}(T)) = Ln(k_{II}^0) - \frac{E_{II}}{R.T} \qquad \text{Equation 2}$$

where k_{II}^0 is the frequency factor, E_{II} the apparent activation energy, R the gases constant and T the absolute temperature. The activation energy of the growth of Layer II, calculated from the slope of this data, was found to be 260±30 kJ.mol^{-1}. The frequency factor k_{II}^0 was estimated at 8.5×10^8 μm^4.s^{-1}. The curve fits corresponding to the fourth-power laws, which are plotted in Figure 6-b, show a good the agreement with the experimental values for durations up to 1800 s. From these results, it was estimated that the growth of SiC crystals occurs only after 61 s at 1450°C, 60 s at 1500°C and 27 s at 1550°C, this delayed time corresponding to the prerequisite carbon saturation of the liquid.

3.3 Pore conversion

During the infiltration of molten silicon, the reaction between the liquid and carbon induces the formation of SiC, not only at the solid/liquid interface, but also within the pores. This reaction implies the progressive closure of the pores as it implies a volume expansion of the solid phase of about 235%, when considering molar volumes for SiC (V_{SiC}^{mol}) and carbon (V_C^{mol}) equal to 12.452 and 5.298 cm^3.mol^{-1}, respectively. The general calculation of the final volume fraction of SiC in the case of a full conversion can be determined from Equations 3, 4, 5 and 6:

$$V_C^0 + V_{pore} = V_C^f + V_{SiC} = 1 \qquad \text{Equation 3}$$

$$V_{SiC} = \left(V_C^0 - V_C^f\right) \times \frac{V_{SiC}^{mol}}{V_C^{mol}} = V_{pore} + \left(V_C^0 - V_C^f\right) \qquad \text{Equation 4}$$

$$\left(V_C^0 - V_C^f\right) = \frac{V_{pore}}{\frac{V_{SiC}^{mol}}{V_C^{mol}} - 1} \qquad \text{Equation 5}$$

$$V_{SiC} = \frac{V_{pore}}{\left(\frac{V_{SiC}^{mol}}{V_C^{mol}} - 1\right)} \times \frac{V_{SiC}^{mol}}{V_C^{mol}} = \frac{V_{pore}}{\left(1 - \frac{V_C^{mol}}{V_{SiC}^{mol}}\right)} \qquad \text{Equation 6}$$

with, respectively, V_C^0 and V_{pore}, the initial volume fractions of carbon and pores; and V_C^f and V_{SiC} the final volume fractions of carbon and silicon. In the present case, with a measured porosity of 11%, the expected final volume fraction of SiC is estimated to be equal to 19.2%. The variations of the conversion percentage, i.e. the SiC surface fraction in the substrate are plotted in Figure 7-a. The experimental values, estimated from image analysis by using ImageJ software, were determined from the whole thickness of the infiltrated areas. The conversion ratio increases quickly up to values close to - but below - the theoretical value. Cartography of the present phases were obtained from image treatments based on the different grey contrast of the present phases. In a general manner, it can be noted that the precipitation of SiC crystals within the pores starts from early steps of the treatment, as visible in Figure 7-a. The kinetics of the formation of SiC crystals at 10 s shown in the inset of Figure 7-a appears to be activated by the temperature. The variations at longer durations are more complex. In a general manner, the conversion percentage quickly increases up to 60 s to reach values between 14.1 and 17.5%. Beyond this duration, the conversion ratio at 1450°C varies only slightly and even tend to decrease because of the silicon flow depletion at the tip of the infiltration front. Consequently, the pores are not fully converted and the front becomes irregular. This phenomenon is particularly marked at 1550°C. Once again, the samples exhibit a particular behavior at 1500°C. The above-mentioned effect is still present but occurs only after a resumption of the conversion after 300 s. This could be correlated to the rapid progression of the infiltration length, as identified in Figure 4-a. The progression of the liquid at this temperature appears to be faster and less limited than for the two other temperatures, resulting in a lower conversion ratio of the infiltrated area up to 300 s. Once the liquid infiltration kinetics have decreased, the conversion rate increases. This case is of interest as the infiltration front is the deepest and the degree of conversion the highest. The variations observed in the Figure 7-a between 300 and 600 reveal that the infiltration fronts become less

and less regular during the infiltration process: less and less areas in the newly infiltrated zone are filled. That is why the converted surface percentages decrease between 300 and 600s. The point at 1500°C for 300s is more surprising, the expected value would be closer to 20% than 15%. But this fact reveals probably the effect of the local porous network which can be more or less interconnected, what affects the progress of the infiltration front. The BSE images of areas comprised between the solid/liquid interface and a maximum depth of 100 μm were also analyzed with ImageJ software to estimate the kinetic evolution of the pores' conversion, the full conversion corresponding to the filling of the pores by SiC. The results of this analysis are shown in Figure 7-b. The curves exhibit the same shape with a rapid increase of the pore conversion (called α) up to 300 s, leading to values comprised between 77 and 99%, the latter being obtained at 1550°C. The subsequent evolution is slower, as a full conversion is observed for durations of 600 s at 1500°C or 1200 s at 1450°C. This is in good agreement with the slow progress of the infiltration length, as noticed above for longer durations (Fig. 4-a). This also means that a residual flow of liquid silicon still remains through tiny channels winding between SiC crystals. It is worth noting that the pore filling by SiC occurs by precipitation of SiC crystals equally in contact with carbon or at the center of the pore, i.e. within the liquid. In order to identify the limiting mechanism regulating the pores conversion and consequently their closure, usual kinetic models of the solid-state reactions were considered [35]. These models are basically divided into three main categories: 1) models where the reaction rate is determined by nucleation and growth; 2) models in which the controlling step is the diffusion of reactants; 3) models where the mechanism is ruled by the chemical reaction at the reactant-product interface. The most appropriate kinetic models $g(\alpha) = k.t$ are listed in Table 1. Among these models, the best fitting of the experimental data was obtained for D3 three-dimensional diffusion model for a spherical symmetry corresponding to Equation 7:

$$\left(1-(1-\alpha)^{\frac{1}{3}}\right)^2 = k_{pore}(T).t \qquad \text{Equation 7}$$

with α the conversion degree of the pores, k_{pore} the kinetic coefficient at the temperature T and t the time. Data fittings with D3 model functions are shown in Figure 7-c, for which only the α values lower than 1 were considered. All the correlation factors exceed 98%. The Arrhenius plot presented in Figure 7-d was drawn based on the law expressed by Equation 8:

$$Ln\left(k_{pore}(T)\right) = Ln\left(k^0_{pore}\right) - \frac{E_{pore}}{R.T} \qquad \text{Equation 8}$$

where k_{pore} is the frequency factor, E_{pore} the apparent activation energy, R the gases constant, and T the absolute temperature. From the slope of this curve, the activation energy of the kinetics of the pore filling by SiC was found to be 320±40 kJ.mol^{-1}. The corresponding frequency factor k_{pore} was estimated at 3.3×10^6 s^{-1}. The curves of D3 laws are plotted in Figure 7-b. A satisfying agreement is obtained between the calculated values and the experimental ones. Raman spectroscopy mappings were also recorded from porous regions located near the silicon/carbon interface or further in the bulk. For a very short time (10 s), almost only the cubic silicon features (strong optical phonon at 520 cm^{-1} and weak 2TA and 2TO modes at 308 and 930-1000 cm^{-1}, respectively) can be noticed on the spectra from the outer surface (Fig. 8) or the pores. Traces of β-SiC are only found in the pores near the surface, as shown by the optical micrographs and confirmed by the very weak transverse optical (TO) phonon around 800 cm^{-1} [36]. After 60 s, SiC is still almost absent at the surface but large β-SiC grains have grown within the pores, involving stacking faults as indicated by the large and asymmetric TO peak. After 300 s, large faulty β-SiC grains appeared at the surface (Fig. 9). The optical micrograph and the Raman mapping confirm that the pores close to the surface are almost filled with SiC (Fig. 9). Yet, the Si peak remains very strong all across the pore section, indicating that molten silicon efficiently feed the reaction with the carbon substrate. The spectra exhibit a clear Fano shape of main Si peak (asymmetric, broadened and downshifted in frequency compared to the original peak) as well as local modes at 620 and 640 cm^{-1}, which are typical of boron (p type) doping (Fig. 10) [37,38]. The B is likely introduced in the melt from the BN coating used to prevent wetting. The B

concentration in the Si melt (outside the carbon material) gradually increases with the contact time as shown by the strong enhancement of the Fano shape and the local modes (Fig. 11). The Raman analysis also reveals that a B depletion appears between the outside and the core of the porous material (Fig. 10). The origin of such a gradient is not fully explained yet. It could be related to the reaction between carbon and liquid silicon and the development of a reverse C concentration profile. The β-SiC features also vary significantly with the reaction time and the penetration distance in the pores. As expected, the SiC-TO peak intensity increases with respect to that the main Si peak, due to the higher SiC conversion rate. The structural organization of the β-SiC phase also improves from the pores located near the outer surface to those in core, as shown by the sharper TO and LO components (Fig. 10). As expected for pure crystalline β-SiC, the optical phonons are both sharp and intense in the SiC spectra recorded from core. In contrast, the TO component is broader, asymmetric (even sometimes split) while the LO peak much less intense or completely absent for the SiC regions near the surface (Fig. 10). These changes are likely related to a strong level of doping or internal stresses in the β-SiC phase near the surface of the specimen and decreasing in the bulk. If the vanishing of the LO peak of β-SiC has been related to a high concentration of n dopant (e.g. with nitrogen) [39], the nature of dopant(s) responsible for such a combination of effects remains uncertain. Further physicochemical investigations would be necessary for a better understanding.

3.4 Discussion

The results from this study confirm globally the mechanisms previously proposed by J.C. Margiotta et al. [40] for LSI process. The evolution of the samples can be summarized in three main steps consisting of:

1) a rapidly spreading and infiltration of liquid silicon with, in parallel, a rapid carbon dissolution in the liquid. This stage proceeds until at least 600 seconds before stabilization,

2) the very quick growth of β-SiC crystals in the pores, followed by a grain growth at the outer surface of the carbon substrate after approximately 30 seconds at 1550°C or 60 seconds at 1450°C,

3) finally, the completion of a continuous and almost stabilized SiC layer at the surface of carbon substrate from 1200 to 1800 seconds and, in the same time, the filling of the pores by SiC from 400 to 1100 seconds, both processes being controlled by diffusion.

All these steps are clearly promoted by an increase in the temperature. The BSE image analyses realized on the samples confirm that the infiltrating kinetic follow a logarithmic law up to 600 seconds with a strong decrease of the wetting angle at the surface of carbon substrate eventually leading to values lower than 20°. The particular behavior observed at 1500°C must be noted. At this temperature, accelerated spreading and infiltration kinetics are measured for the first 60 seconds, as compared to the two other temperatures. This particular behavior of the liquid at 1500°C is probably related to a synergism between the carbon saturation of the liquid and the germination/growth kinetic of the SiC crystals at the surface and within the substrate. It was estimated herein that the delay of SiC formation at the surface of the substrate at 1500°C is close to the delay at 1450°C, i.e. ~60 seconds. This behavior may be justified by a lower increase with temperature of the dissolution kinetics than the carbon-solubility. The duration of carbon dissolution may thus be prolonged with regard to the others temperatures, promoting both wetting and infiltration. The reaction layer was also found to be composed of two sublayers: layer I, composed of nanometric SiC crystals and free silicon and layer II, made of larger and facetted SiC crystals. This work confirms that the growth kinetics of the SiC layer follow a fourth-power law. The k_{II} kinetic coefficients obtained here and reported by H. Zhou et al. [29] are given in Table 2. One can notice that the values from the present work are approximately 10 times larger. Such a strong difference can be justified by the nature of the carbon sources. H. Zhou et al., who only considered the wetting and the reaction at the surface choose a dense glassy carbon instead of the porous graphitic carbon of the current study. It is well known that the SiC growth is slower from glassy carbon than from

graphitic carbon [16]. This fact is confirmed here but it is interesting to note that a fourth-power law can be applied in both cases. Such a time function is unusual and reveals a specific growth mechanism of the SiC crystals, which appears strongly limited by a particular diffusion mechanism as already proposed by H. Zhou et al.. The conversion of the pores located just below the surface to SiC follows a classical D3 law corresponding to a limitation by volume diffusion. The comparison between the experimental and calculated values for the infiltration depth, surface SiC growth and pore conversion is shown in Figure 12. In all cases a satisfying agreement is obtained up to 1800 seconds, the further evolutions being very limited. From these results it can be deduced that the infiltration of molten silicon is a very fast process which is clearly limited by the formation of SiC crystals. In the present case, the infiltration depths are relatively modest since close to 1 mm. The main purpose of this work was to obtained characteristic values and laws for a given model carbon material. Following works will be focused on others types of carbon samples exhibiting different porous structures and/or varieties of sp^2 carbon. By this way, the effects of these parameters will be more clearly identified and understood with the aim of promoting both the infiltration capability and the synthesis of pure and dense silicon carbide ceramics.

4. Conclusion

LSI reactions were carried out on graphitic carbon with an open porosity of only 11% and a narrow pore size distribution. The heating treatments were performed at 1450, 1500 or 1550°C for time durations of 10, 60, 300, 600, 1200, 1800 and 3600 seconds, at high heating and cooling rates (300°C.min^{-1}). The shortest isothermal durations were helpful to evidence and measure the fastest phenomenon taking place. BSE images were analyzed to examine the behavior of molten silicon at the surface and within the carbon substrate but also to quantify the kinetics of the SiC formation at the surface and within the pores. Rapid spreading and infiltration of molten silicon are observed from the first 60 seconds. At least half of the maximal infiltration depths are reached only after 60 seconds of heating. This indicates that

the progress of the phenomenon is intrinsically favorable. The limiting factor is not the viscous flow of silicon but rather the chemical reaction between carbon and liquid silicon at the reaction front located at the surface and in the pores of the carbon substrate. The kinetics of the SiC layer growth at the surface of the substrate and the kinetics of the pores closure were consequently determined. The growth rate of the SiC layer from graphitic carbon was found to obey a fourth-power law, as reported for glassy carbon, the kinetics measured for graphitic carbon being significantly higher. The corresponding activation energy was estimated at 260±30 $kJ.mol^{-1}$. The kinetic of pore filling by SiC obeys a D3 model corresponding to a control by volume diffusion with an activation energy equal to 320±40 $kJ.mol^{-1}$. Raman spectroscopy reveals that the formed SiC grains are only of β–type and shows an improvement of their structural organization from the pores located near the outer surface to those in core. A strong level of doping or internal stresses near the surface of the specimen and decreasing in the bulk was also evidenced for the formed β-SiC grains. These results should be useful for the optimization of LSI process through a better control of SiC formation.

Acknowledgement

The authors wish to thank Laurine Lapuyade and Muriel Alrivie, from the Laboratory of ThermoStructural Composites (LCTS - UMR 5801 - UB-CNRS-CEA-SAFRAN), for their kind assistance.

References

[1] R. Voytovych, V. Bougiouri, N.R. Calderon, J.Narciso, N. Eustathopoulos, Reactive infiltration of porous graphite by NiSi alloys, Acta Mater. 56 (2008) 2237-2246. https://doi.org/10.1016/j.actamat.2008.01.011

[2] N.R. Calderon, M. Martinez-Escandell, J. Narciso, F. Rodriguez-Reinoso, The role of carbon biotemplate density in mechanical properties of biomorphic SiC, J. Eur. Ceram. Soc. 29 (2009) 465-472. https://doi.org/10.1016/j.jeurceramsoc.2008.05.049

[3] N.R. Calderon, M. Martinez-Escandell, J. Narciso, F. Rodriguez-Reinoso, Manufacture of Biomorphic SiC Components with Homogeneous Properties from Sawdust by Reactive Infiltration with Liquid Silicon, J. Am. Ceram. Soc. 93 (2010) 1003-1009. https://doi.org/10.1111/j.1551-2916.2009.03572.x

[4] H. Matsunami, T. Kimoto, Step-controlled epitaxial growth of SiC: High quality homoepitaxy, Mater. Sci. Eng. R20 (1997) 125-166. https://doi.org/10.1016/S0927-796X(97)00005-3

[5] R.W. Rice, Ceramic Processing: An overview, AlChE Journal 36 (1990) 481-510. https://doi.org/10.1002/aic.690360402

[6] N.D. Shcherban, Review on synthesis, structure, physical and chemical properties and functional characteristics of porous silicon carbide, J. Ind. Eng. Chem. 50 (2017) 15-28. https://doi.org/10.1016/j.jiec.2017.02.002

[7] A. Maity, H. Das, D. Kalita, N. Kayal, T. Goswami, O. Chakrabarti, Studies on formation and siliconization of carbon template of coir fibreboard precursor to SiC ceramics, J. Eur. Ceram. Soc. 34 (2014) 3499–3511. https://doi.org/10.1016/j.jeurceramsoc.2014.05.010

[8] G. Bianchi, P. Vassori, B. Vila, G. Annino, M. Nagliati, M. Mallah, S. Gianella, M. Valle, M. Orlandi, A. Ortona, Reactive silicon infiltration of carbon bonded preforms embedded in powder field modifiers heated by microwaves, Ceram. Inter. 41 (2015) 12439–12446. https://doi.org/10.1016/j.ceramint.2015.06.087

[9] Y. Tong, S. Bai, X. Liang, Q.H. Qin, J. Zhai, Reactive melt infiltration fabrication of C/C-SiC composite: Wetting and infiltration, Ceram. Inter. 42 (2016) 17174-17178. https://doi.org/10.1016/j.ceramint.2016.08.007

[10] Q. Zhong, X. Zhang, S. Dong, J. Yang, J. Hu, L. Gao, P. He, H. Zhou, Z. Wang, Y. Ding, Reactive Melt Infiltrated Cf/SiC Composites with robust matrix derived from novel engineered pyrolytic carbon structure, Ceram. Inter. 43 (2017) 5832-5836. https://doi.org/10.1016/j.ceramint.2017.01.089

[11] P. Sangsuwan, J.A. Orejas, J.E. Gatica, S.N. Tewari, M. Singh, Reaction-Bonded Silicon Carbide by Reactive Infiltration, Ind. Eng. Chem. Res. 40 (2001) 5191-5198. https://doi.org/10.1021/ie001029e

[12] R. Pampuch, E. Walasek, J. Bialoskbrski, Reaction mechanism in carbon-liquid silicon systems at elevated temperatures, Ceram. Inter. 12 (1986) 99-106. https://doi.org/10.1016/0272-8842(86)90023-4

[13] R. Pampuch, J. Bialoskbrski, E. Walasek, Mechanism of reactions in the Si_l+ C_f system and the self-propagating high-temperature synthesis of silicon carbide, Ceram. Inter. 13 (1987) 63-68. https://doi.org/10.1016/0272-8842(87)90039-3

[14] H. Zhou, R.N. Singh, Kinetics model for the growth of silicon carbide by reaction of liquid silicon with carbon, J. Am. Ceram. Soc. 78 (1995) 2456-2462. https://doi.org/10.1111/j.1151-2916.1995.tb08685.x

[15] R. Deike, K. Schwerdlfeger, Reactions between liquid silicon and different refractory materials, J. Electrochem. Soc. 142 (1995) 609-614. https://doi.org/10.1149/1.2044109

[16] A. Favre, H. Fuzellier, J. Suptil, An original way to investigate the siliconizing of carbon materials, Ceram. Inter. 29 (2003) 235-243. https://doi.org/10.1016/S0272-8842(02)00110-4

[17] A. Maity, D. Kalita, T.K. Kayal, T. Goswami, O. Chakrabarti, H.S. Maiti, P.G. Rao, Synthesis of SiC ceramics from processed cellulosic bio-precursor, Ceram. Inter. 36 (2010) 323-331. https://doi.org/10.1016/j.ceramint.2009.09.006

[18] R. Voytovych, R. Israel, N.Calderon, F. Hodaj, N. Eustathopoulos, Reactivity between liquid Si or Si alloys and graphite, J. Eur. Ceram. Soc. 32 (2012) 3825–3835. https://doi.org/10.1016/j.jeurceramsoc.2012.05.020

[19] J.C. Margiotta, D. Zhang, D.C. Nagle, C.E. Feeser, Formation of dense silicon carbide by liquid silicon infiltration of carbon with engineered structure, J. Mater. Res. 23 (2008) 1237-1248. https://doi.org/10.1557/JMR.2008.0167

[20] E.O. Einset, Capillary Infiltration Rates into Porous Media with Applications to Silcomp Processing, J. Am. Ceram. Soc. 79 (1994) 333-338. https://doi.org/10.1111/j.1151-2916.1996.tb08125.x

[21] P. Sangsuwan, N.S. Tewari, J.E. Gatica, M. Singh, R. Dickerson, Reactive infiltration of silicon melt through microporous amorphous carbon preforms, Metall. Mater. Trans. B30 (1999) 933-944. https://doi.org/10.1007/s11663-999-0099-1

[22] O. Dezellus, S. Jacques, F. Hodaj, N. Eustathopoulos, Wetting and infiltration of carbon by liquid silicon, J. Mater. Sci. 40 (2005) 2307-2311. https://doi.org/10.1007/s10853-005-1950-7

[23] N. Eustathopoulos, Dynamics of wetting in reactive metal ceramic systems, Acta Mater. 46 (1998) 2319-2327. https://doi.org/10.1016/S1359-6454(98)80013-X

[24] O. Dezellus, F. Hodaj, N. Eustathopoulos, Chemical reaction limited spreading: The triple line velocity versus contact angle relation, Acta Mater. 50 (2002) 4741-4753. https://doi.org/10.1016/S1359-6454(02)00309-9

[25] N. Eustathopoulos, R. Israel, B. Drevet, D. Camel, Reactive infiltration by Si: Infiltration versus wetting, Scripta Mater. 62 (2010) 966-971. https://doi.org/10.1016/j.scriptamat.2010.02.030

[26] Y.M. Chiang, R.P. Messner, C.D. Terwilliger, D.R. Behrendt, Reaction-formed silicon-carbide, Mater. Sci. Eng. A-Struct. Mater. Prop. Microstruct. Proc. 144 (1991) 63-74. https://doi.org/10.1016/0921-5093(91)90210-E

[27] S. Safi, R.Y. Rad, In situ synthesis of nano size silicon carbide and fabrication of C–SiC composites during the siliconization process of mesocarbon microbeads preforms, Ceram. Inter. 38 (2012) 5081–5087. https://doi.org/10.1016/j.ceramint.2012.03.010

[28] B. Mainzer, K. Kelm, P. Watermeyer, M. Freiß, D. Koch, How to tame the aggressiveness of liquid silicon in the LSI process, Key Eng. Mater. 742 (2017) 238-245. https://doi.org/10.4028/www.scientific.net/KEM.742.238

[29] H. Zhou, R.N. Singh, Kinetics model for the growth of silicon carbide by the reaction of liquid silicon with carbon, J. Am. Ceram. Soc. 78 (1995) 2456-2462. https://doi-org/10.1111/j.1151-2916.1995.tb08685.x

[30] Y. Wang, S. Tan, D. Jiang, The effect of porous carbon preform and the infiltration process on the properties of reaction-formed SiC, Carbon 42 (2004) 1833-1839. https://doi.org/10.1016/j.carbon.2004.03.018

[31] C.A. Schneider, W.S. Rasband, K.W. Eliceiri, NIH Image to ImageJ: 25 years of image analysis, Nature methods 9 (2012) 671-675. https://doi.org/10.1038/nmeth.2089

[32] E.S. Nelson, P. Colella, Parametric Study of Reactive Melt Infiltration, Report No. NASA TM-2000-209802, Hanover, MD, 2000. https://ntrs.nasa.gov/archive/nasa/casi.ntrs.nasa.gov/20000034033.pdf

[33] F.H. Gern, R. Kochendorfer, Liquid silicon infiltration: Description of infiltration dynamics and silicon carbide formation, Composites Part A-Appl. Sci. Manuf. 28 (1997) 355-364. https://doi.org/10.1016/S1359-835X(96)00135-2

[34] E.O. Einset, Analysis of reactive melt infiltration in the processing of ceramics and ceramic composites, Chem. Eng. Sci. 53 (1998) 1027-1039. https://doi.org/10.1016/S0009-2509(97)00379-5

[35] A. Khawam, D.R. Flanagan, Solid-State kinetic models basics and mathematical fundamentals, J. Phys. Chem. B110 (2006) 17315-17328. https://doi.org/10.1021/jp062746a

[36] D. W. Feldman, J. H. Parker, Jr., W. J. Choyke, L. Patrick, Phonon dispersion curves by Raman scattering in SiC, polytypes 3C, 4H, 6H, 15R, and 21R, Phys. Rev. 173 (1968) 787-793. https://doi.org/10.1103/PhysRev.173.787

[37] F. Cerdeira, T.A. Fjeldly, M. Cardona, Effect of Free Carriers on Zone-Center Vibrational Modes in Heavily Doped p-type Si. II. Optical Modes, Phys. Rev. B8 (1973) 4734-4745. https://doi.org/10.1103/PhysRevB.8.4734

[38] F. Cerdeira, T.A. Fjeldly, M. Cardona, Raman study of the interaction between localized vibrations and electronic excitations in boron-doped silicon, Phys. Rev. B9 (1974) 4344-4350. https://doi.org/10.1103/PhysRevB.9.4344

[39] H. Yugami, S. Nakashima, A. Mitsuishi, A. Uemoto, M. Shigeta, K. Furukawa, A. Suzuki, S. Nakajima, Characterization of the free□carrier concentrations in doped β□SiC crystals by Raman scattering, J. Appl. Phys. 61 (1989) 354-358. https://doi.org/10.1063/1.338830

[40] J.C. Margiotta, D. Zhang, D. C. Nagle, Microstructural evolution during silicon carbide (SiC) formation by liquid silicon infiltration using optical microscopy, Int. Journal of Refractory Metals & Hard Materials 28 (2010) 191-197. https://doi.org/10.1016/j.ijrmhm.2009.09.002

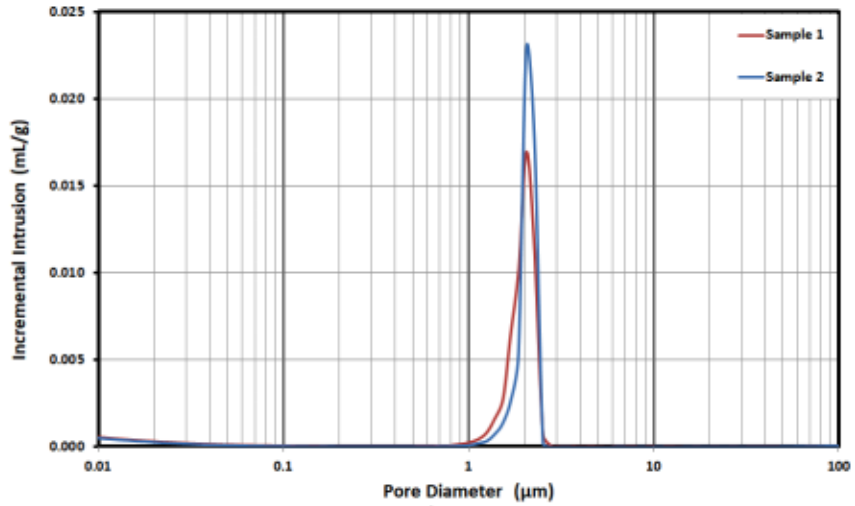

a)

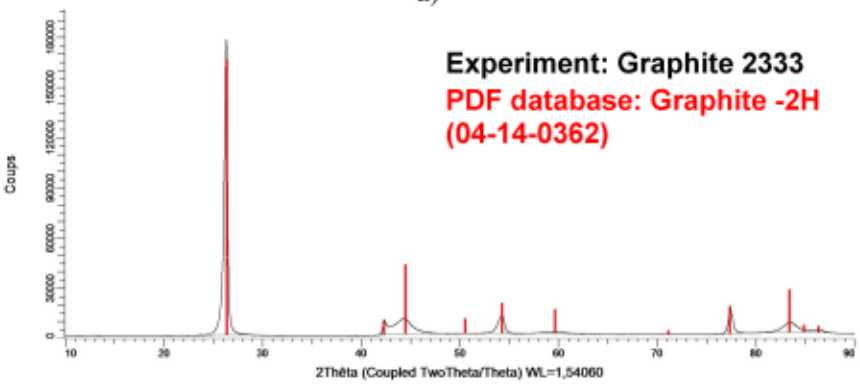

b)

Figure 1. Analysis of starting graphite 2333: a) pore-size distribution measured on two samples, b) X-ray diffraction pattern.

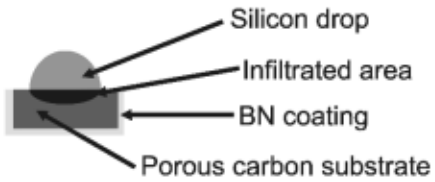

Figure 2. Experimental setup for the infiltration experiments of molten silicon in graphite.

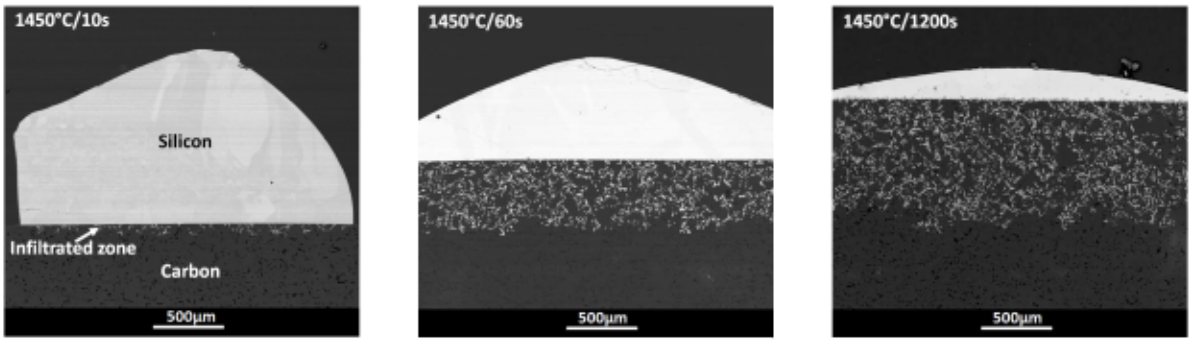

a) b) c)

Figure 3. BSE images of the infiltrated zones at 1450°C produced in: a) 10 seconds, b) 60 seconds, and c) 1200 seconds.

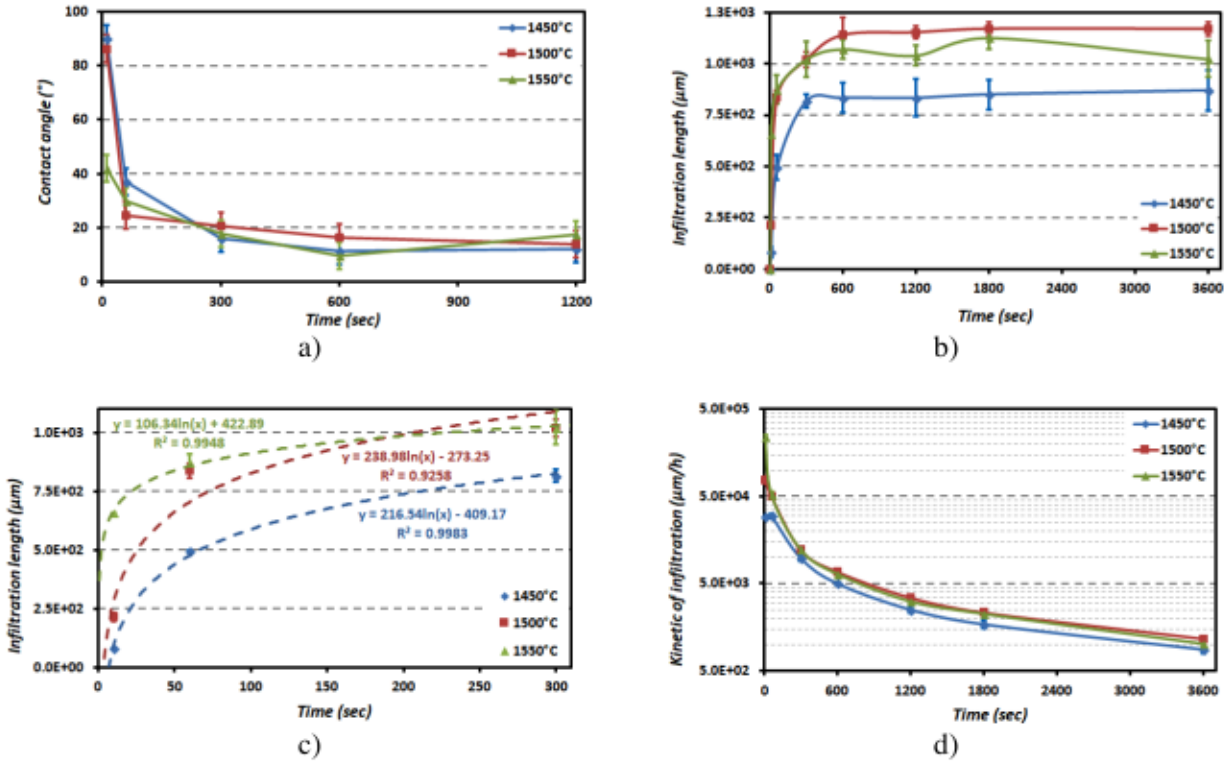

Figure 4. Wetting and infiltration of liquid silicon at 1450, 1500 and 1550°C versus time: a) contact angle observed at the surface of C/Si samples, b), experimental infiltration lengths, c) logarithmic fittings of the infiltration length for short durations, and d) apparent infiltration kinetics.

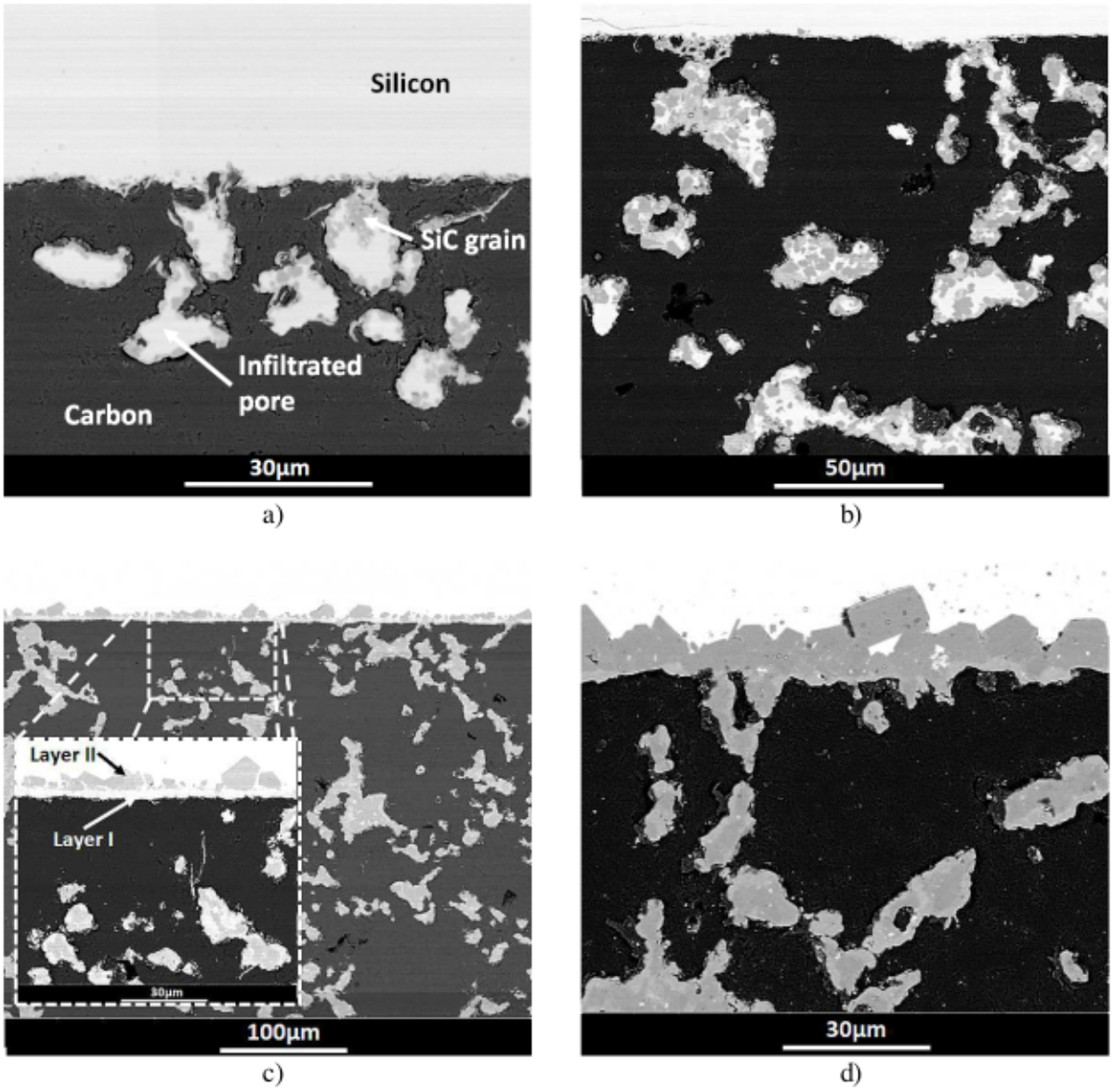

Figure 5. BSE micrographs of Si-infiltrated graphite samples after heating at 1450°C after: a) 10 s, b) 60 s, c) 300 s; and d) 600 s.

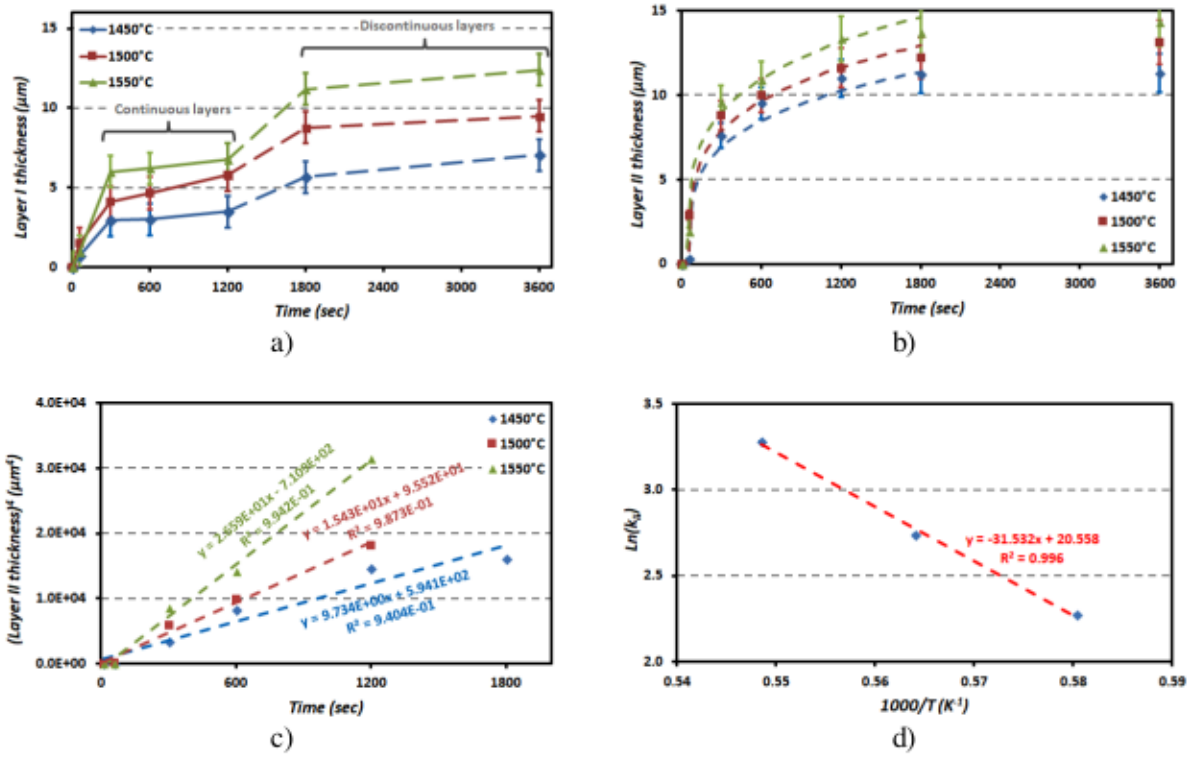

Figure 6. Reaction zone at the substrate/liquid interface: a) thickness evolution of Layer I and plots of the fourth-power laws, b) evolution of Layer II, c) fit of Layer II thicknesses with a fourth-power law, and d) Arrhenius plot of the growth rate of Layer II.

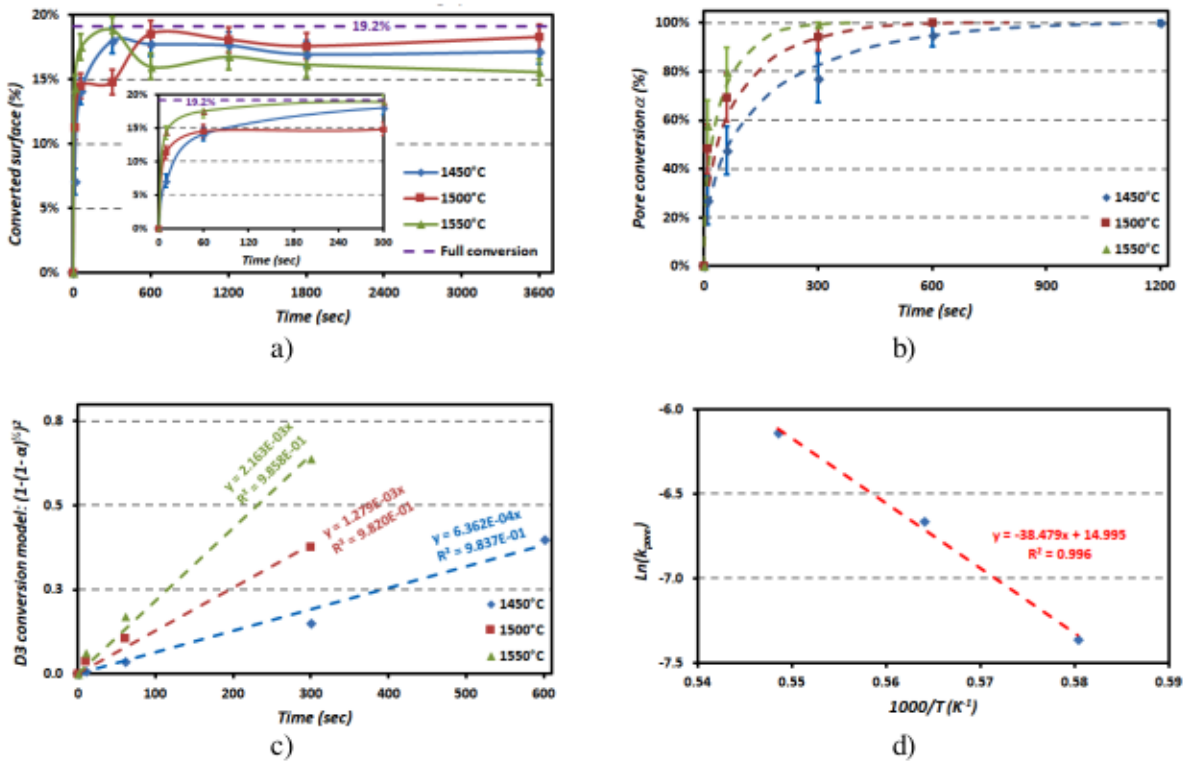

Figure 7. Reaction zone within the pores of the substrate: a) evolution of the overall conversion percentage of the infiltrated area (in insert, focus on short durations), b) evolution of pore conversion percentages and plots of the D3 laws, c) fit of the pores conversion ratios with D3 law, and d) Arrhenius plot of the role of pore conversion.

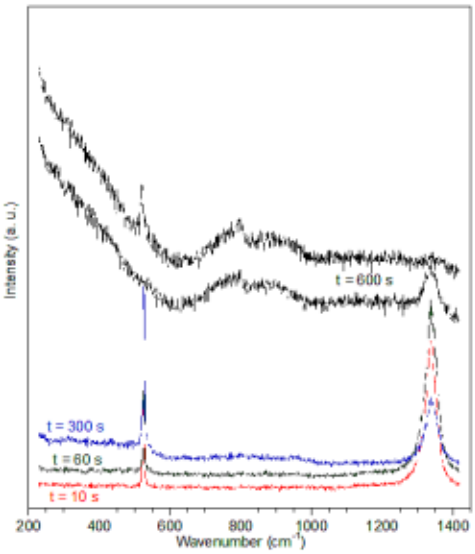

Figure 8. Influence of reaction time on the Raman features: spectra from the outer Si/C interface.

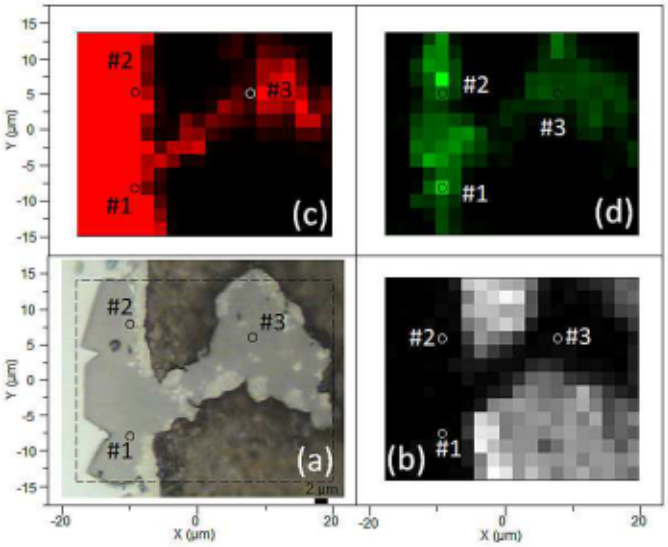

Figure 9. Raman spectroscopy mapping of the near surface region at 300 s of reaction time: (a) optical micrograph, (b) carbon (d) band, (c) Si, and (d) SiC-TO peak intensities.

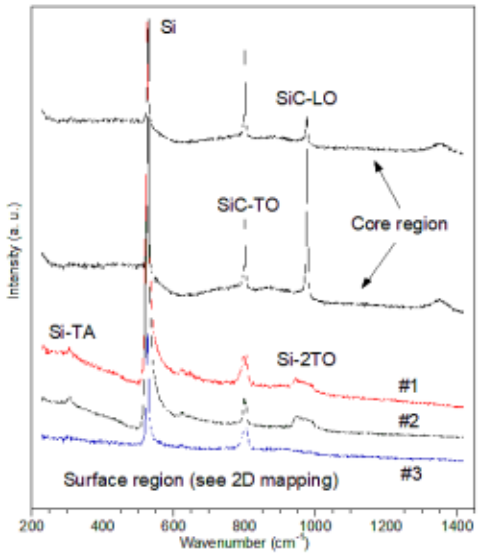

Figure 10. Raman spectra from near surface (#1-3) and the core region of the specimen at 300 s of reaction time.

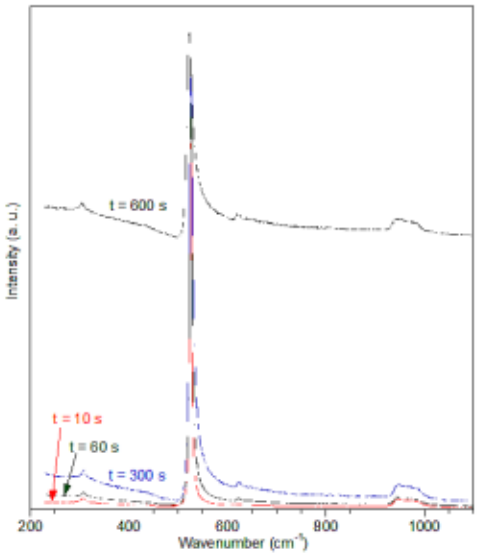

Figure 11. Influence of reaction time on the Raman features: spectra from the Si-alloy.

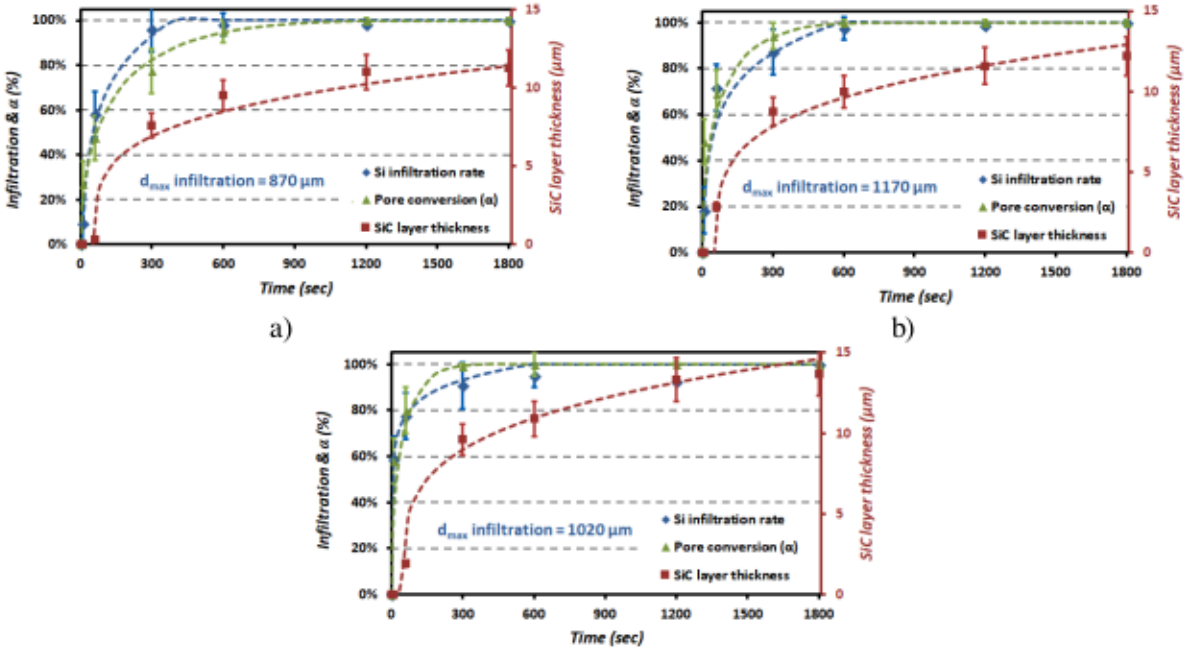

Figure 12. Experimental values (symbols) and calculated curves (dotted lines) of the kinetics of infiltration (%), pore conversion (%) and SiC layer thickness (μm) at: a) 1450°C, b) 1500°C, and c) 1550°C.

Table 1: Customary kinetic models [35]

	Kinetic models	g(α)	Code
Nucleation-growth	Random nucleation and subsequent growth	$[-\ln(1-\alpha)]^{1/2} = k.t$	*A2*
	Random nucleation and subsequent growth	$[-\ln(1-\alpha)]^{1/3} = k.t$	*A3*
	Random nucleation and subsequent growth	$[-\ln(1-\alpha)]^{1/4} = k.t$	*A4*
Chemical reaction	Phase boundary reaction, cylindrical symmetry	$1-(1-\alpha)^{1/2} = k.t$	*R2*
	Phase boundary reaction, spherical symmetry	$1-(1-\alpha)^{1/3} = k.t$	*R3*
Diffusion model	One-dimensional diffusion	$\alpha^2 = k.t$	*D1*
	Two-dimensional diffusion, cylindrical symmetry	$[(1-\alpha).\ln(1-\alpha)] + \alpha = k.t$	*D2*
	Three-dimensional diffusion, spherical symmetry	$[1-(1-\alpha)^{1/3}]^2 = k.t$	*D3*
	Three-dimensional diffusion, cylindrical symmetry	$1-(2/3).\alpha-(1-\alpha)^{2/3} = k.t$	*D4*

Table 2: SiC layer growth kinetics in this study and from H. Zhou et al. [29]

H. Zhou et al.	Temperature	1430°C	1475°C	1510°C
	k_{II} ($\mu m^4.s^{-1}$)	1.3	1.6	1.4
This study	Temperature	1450°C	1500°C	1550°C
	k_{II} ($\mu m^4.s^{-1}$)	9.7	15.4	26.6